AIAA Paper 2025-2270

Assessment of Externally Applied Magnetohydrodynamic Effects on the Boundary Layer in Shock-Dominated Hypersonic Flows

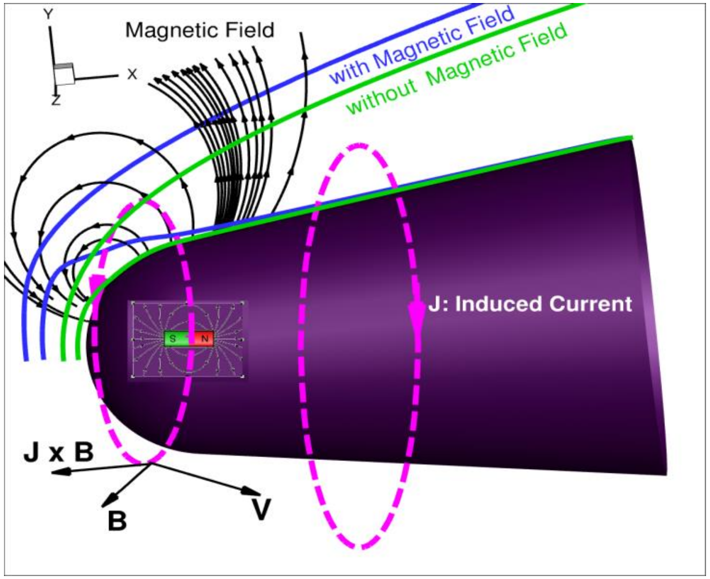

Joseph D. Franciamore and Ozgur Tumuklu

Rensselaer Polytechnic Institute

Hypersonic Aerothermal Vehicle Analysis (HAVA) Laboratory

www.havalab.org

SHAPING THE FUTURE OF AEROSPACE

Motivation

- **Drag reduction** and **thermal management** represent significant challenges in the design of modern strategic hypersonic systems.

- **Magnetohydrodynamic** (MHD) interactions represent a **promising** means of meeting these challenges.

- Aerospace systems experiencing high-enthalpy flow may adopt MHD technology **to enhance attitude control** and vehicular guidance.

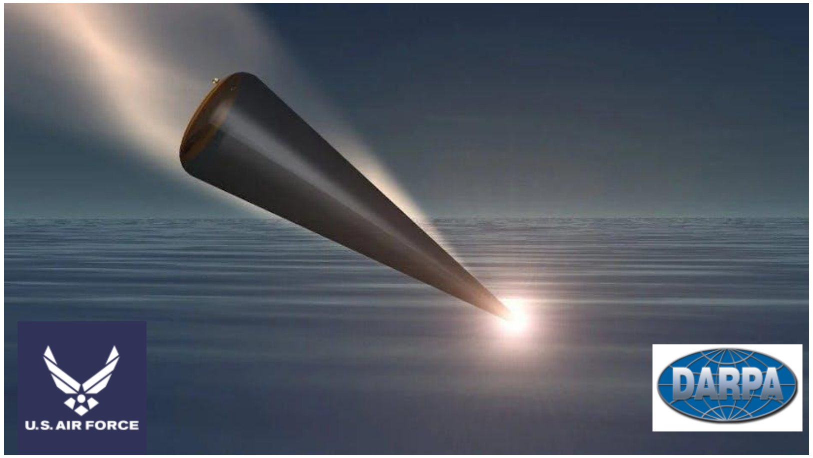

Image from militaryaerospace.com

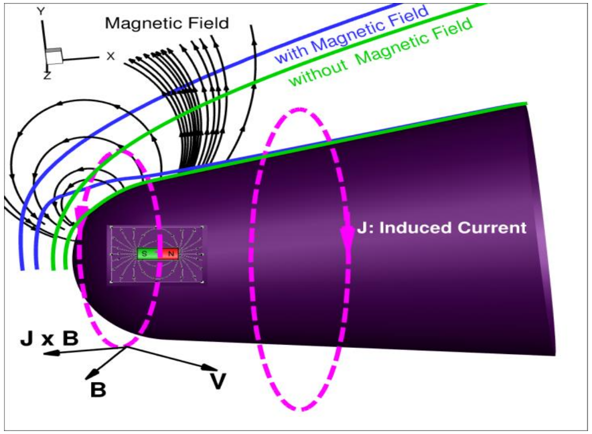

This work aims to:

- investigate the effects **of MHD interactions** in the post shock region, notably in the thick boundary layer.
- characterize the benefits of magnetic external flow control techniques relative to surface **shear stress and heat flux values.**
- determine the feasibility of MHD control techniques as a substitute for traditional methods.

3-D Effects over the 5º-30º Configuration

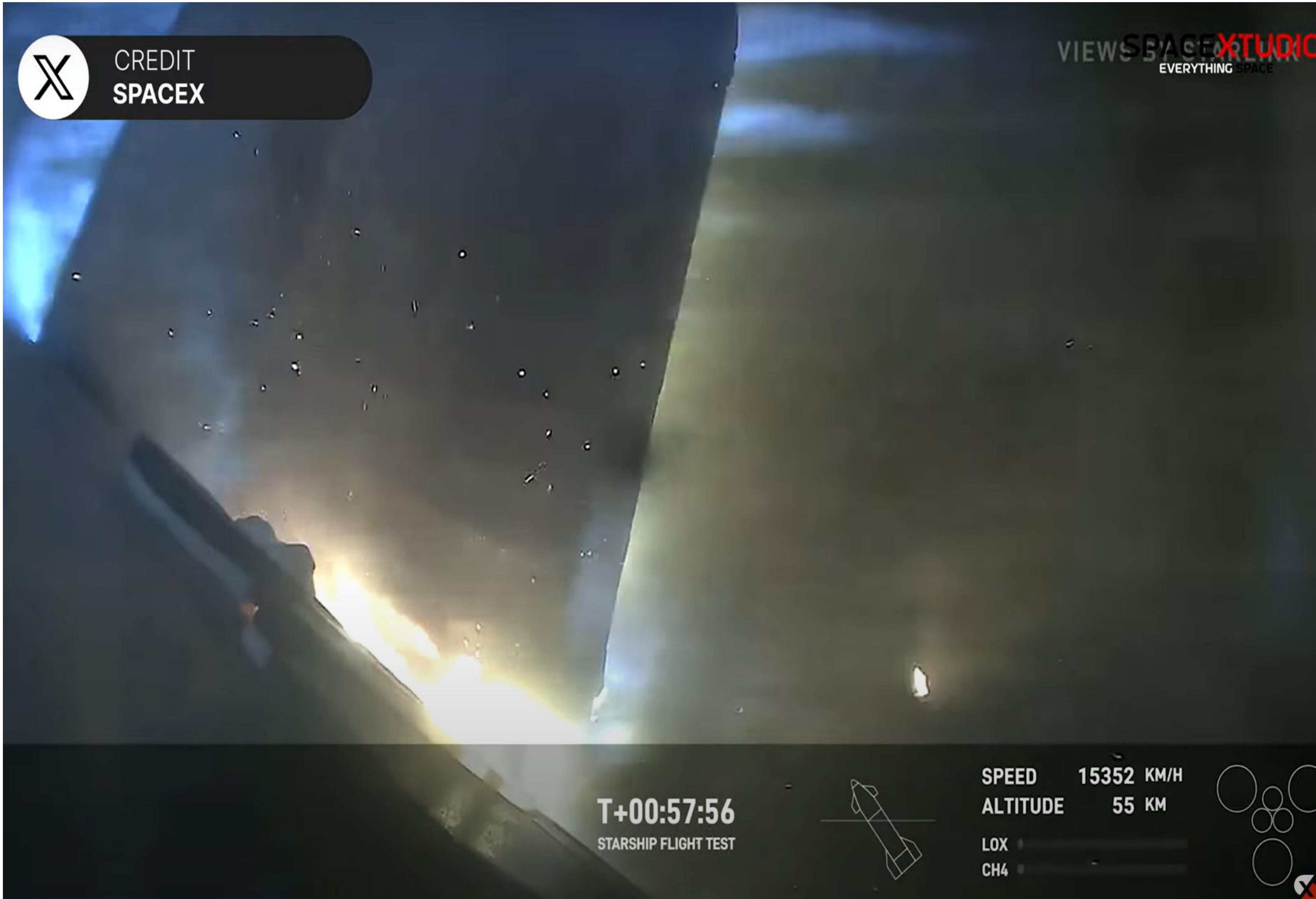

MHD Formulation

$$\frac{\partial \mathcal{U}}{\partial t} + \frac{\partial \left(\mathcal{F}_{i,inv} - \mathcal{F}_{i,vis}\right)}{\partial x_i} - \mathcal{S}_{MHD} = \dot{\mathcal{W}}$$

$$\mathcal{U} = \begin{bmatrix} \rho \\ \rho_s \\ \rho u \\ \rho v \\ \rho w \\ E_{ve} \\ E \end{bmatrix} \quad \mathcal{F}_{i,inv} = \begin{bmatrix} \rho u_i \\ \rho_s u_i \\ \rho u_i u + \delta_{i1} p \\ \rho u_i v + \delta_{i2} p \\ \rho u_i w + \delta_{i3} p \\ E_{ve} u_i \\ (E + p)\, u_i \end{bmatrix} \quad \mathcal{F}_{i,vis} = \begin{bmatrix} 0 \\ -\mathcal{D}_{s,i} \\ \tau_{i1} \\ \tau_{i2} \\ \tau_{i3} \\ -q_{ve,i,m} - e_{ve,m}\mathcal{D}_{m,i} \\ \tau_{ij} u_j - qtr,i - qve,i - \sum_{r \neq e} h_r \mathcal{D}_{r,i} \end{bmatrix} \quad \mathcal{S}_{MHD} = \begin{bmatrix} 0 \\ 0 \\ \left(\vec{\mathbf{J}} \times \vec{\mathbf{B}}\right)_x \\ \left(\vec{\mathbf{J}} \times \vec{\mathbf{B}}\right)_y \\ \left(\vec{\mathbf{J}} \times \vec{\mathbf{B}}\right)_z \\ 0 \\ \vec{\mathbf{V}} \bullet \left(\vec{\mathbf{J}} \times \vec{\mathbf{B}}\right) + \frac{J^2}{\sigma} \end{bmatrix} \quad \dot{\mathcal{W}} = \begin{bmatrix} 0 \\ \dot{\omega}_s \\ 0 \\ 0 \\ 0 \\ \dot{\omega}_{v,m} \\ 0 \end{bmatrix}$$

- In addition to the traditional viscid and inviscid fluxes that are present in the Navier-Stokes equation, an **additional source term** is appended to model MHD effects.
- In each momentum directions, the Lorentz force is present to account for the continuum behavior of current densities subject to magnetic fields generated by the vehicle.
- Misalignment between magnetic forces and the velocity vector, in part due to the separation of charge, constitutes an energy source.
- Joule heating is also added due to the relatively low rates of natural ionization, thereby contributing to electrical resistance.

*Kurganov, A., and Tadmor, E., “New high-resolution central schemes for nonlinear conservation laws and convection–diffusion equations,” Journal of computational physics, Vol. 160, No. 1, 2000, pp. 241–282
OpenCFD Ltd., **OpenFOAM**: The Open Source CFD Toolbox, 2023. URL https://www.openfoam.com, retrieved from https://www.openfoam.com.
Vincent Casseau, An Open-Source CFD Solver for Planetary Entry, Ph.D. Thesis, 2017.

Numerical Schemes and Flow Conditions

Term	Schemes
Time stepping	First order Euler
Fluxes	Kurganov
Gradient	Gauss linear
Divergence	Gauss limited linear
Laplacian	Gauss linear corrected
Interpolation	vanLeer
Surface normal gradient schemes	Grad(U) corrected

Flow Conditions for HEG-I**

Quantity	I
H_o (MJ/kg)	22.4
p_o (MPa)	35.0
T_o (K)	9200
U_∞ (m/s)	5956
p_∞ (Pa)	476
ρ_∞ (kg/m^3)	1.547×10^{-3}
T_∞ (K)	901
p_{p_∞} (kPa)	52.9
M_∞	8.98
$Y[N_2]_\infty$	0.7543
$Y[O_2]_\infty$	0.00713
$Y[NO]_\infty$	0.01026
$Y[N]_\infty$	6.5×10^{-7}
$Y[O]_\infty$	0.2283

Geuzaine, C., and Remacle, J.-F., "**Gmsh**: A 3-D finite element mesh generator with built-in pre- and post-processing facilities," , 2023. URL http://gmsh.info, version 4.9.4

**Knight, Doyle, et al. "Assessment of CFD capability for prediction of hypersonic shock interactions." *Progress in Aerospace Sciences* 48 (2012): 8-26.

Species Mass Fractions

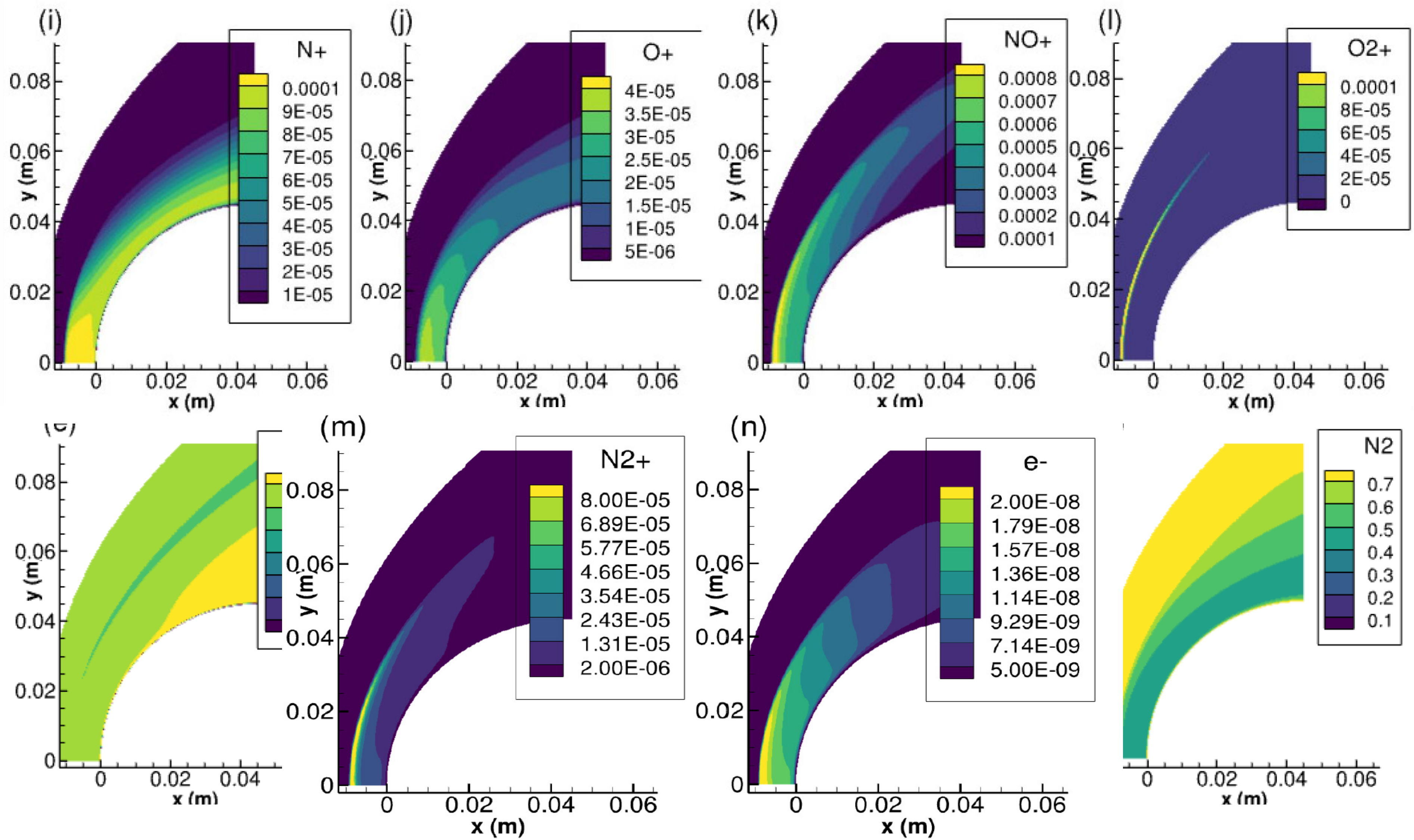

Chemistry Validation and Grid Convergence

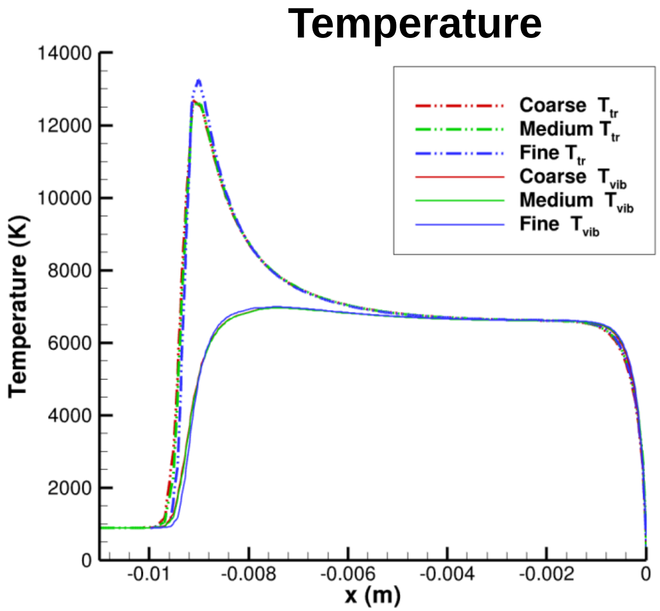

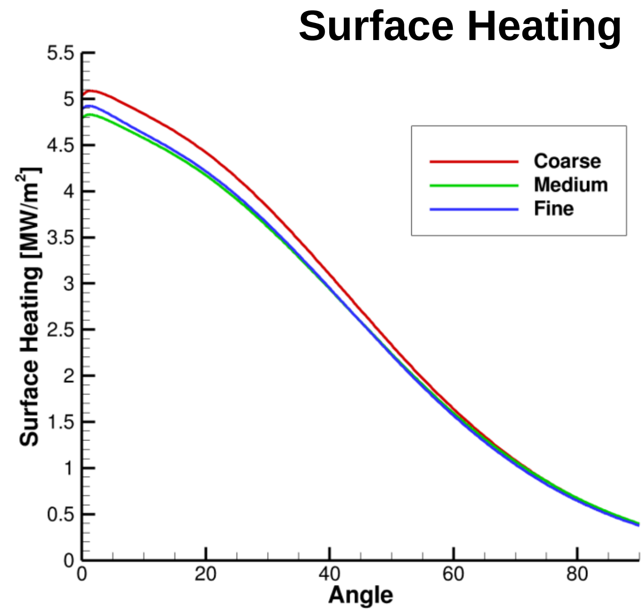

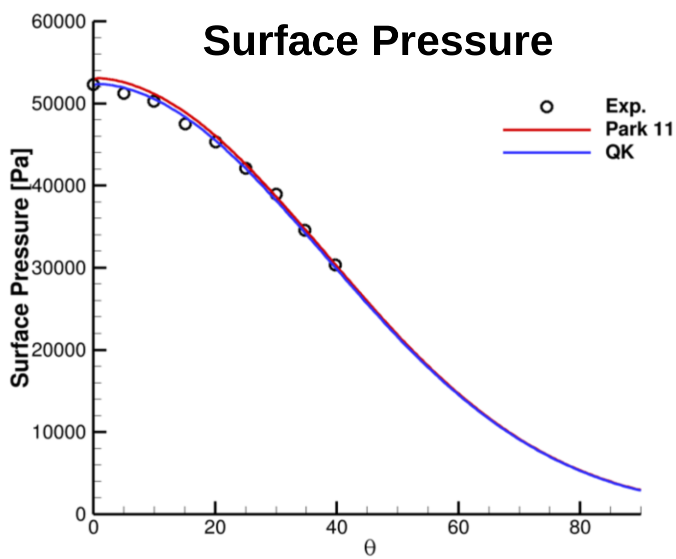

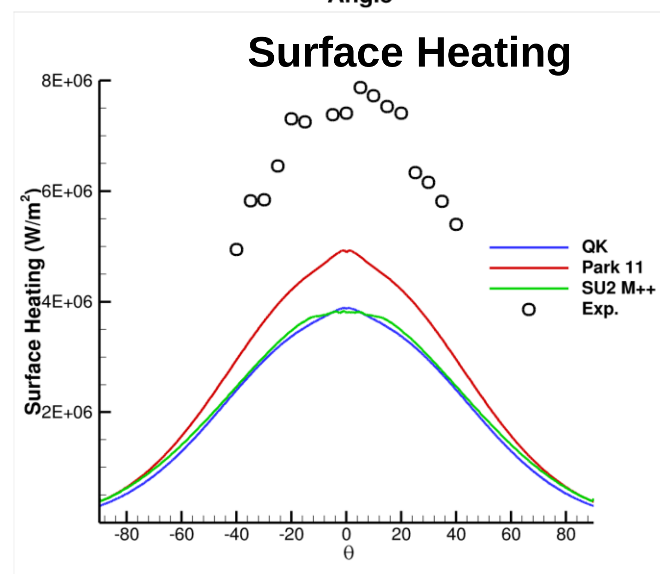

*Karl, S., Martinez Schramm, J., and Hannemann, K., "High enthalpy cylinder flow in HEG: A basis for CFD validation," *33rd AIAA Fluid Dynamics Conference and Exhibit*, 2003, p. 4252.

Configuration and Freestream Conditions*

Flight Envelope

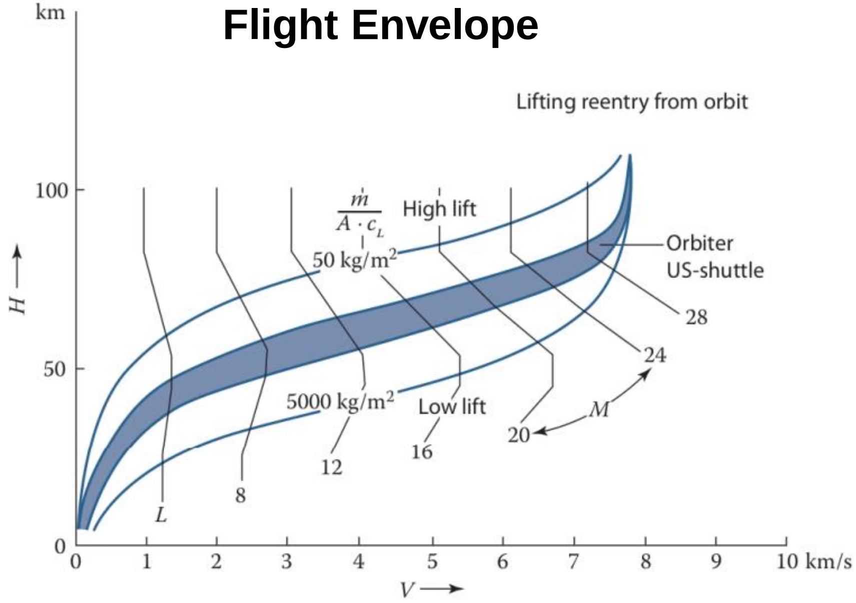

Table 1 Freestream Properties and Conditions

Parameter	Value
p_∞	5.221 Pa
M_∞	25.0
T_∞	219.585 K
T_{wall}	300 K
ρ_∞	8.283×10^{-5} kg/m^3
$\chi_{N_2,\infty}$	0.8
$\chi_{O_2,\infty}$	0.2

Configuration

Flux Scheme	Kurganov
Time Integration	First order Euler
Gradient Schemes	Gauss linear
Divergence Schemes	Gauss limited Linear
Laplacian Schemes	Gauss linear corrected
Interpolation Schemes	Linear Upwind

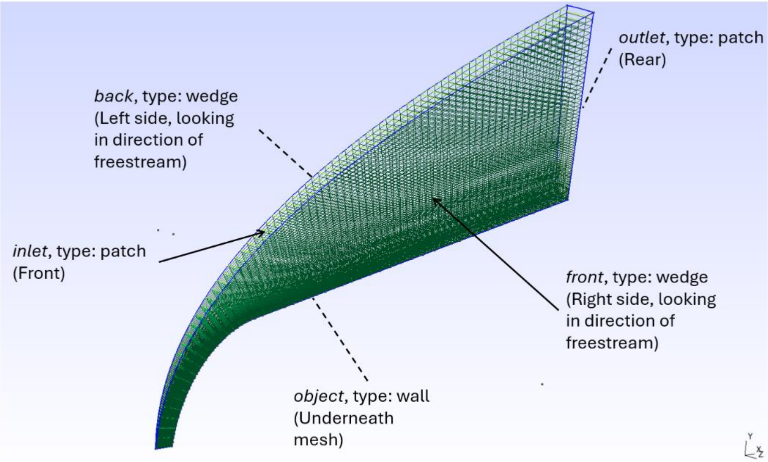

*Hypersonic and High-Temperature Gas Dynamics (AIAA Education)

Geuzaine, C., and Remacle, J.-F., “**Gmsh**: A 3-D finite element mesh generator with built-in pre- and post-processing facilities,” 2023. URL http://gmsh.info, version 4.9.4

Electrical Conductivity Model

- The Hall effect can be neglected for an electrically insulating wall, the Bush temperature-dependent power law was selected to calculate electrical conductivity.
- Data was curve-fit and optimized for the expected temperatures of the simulation.

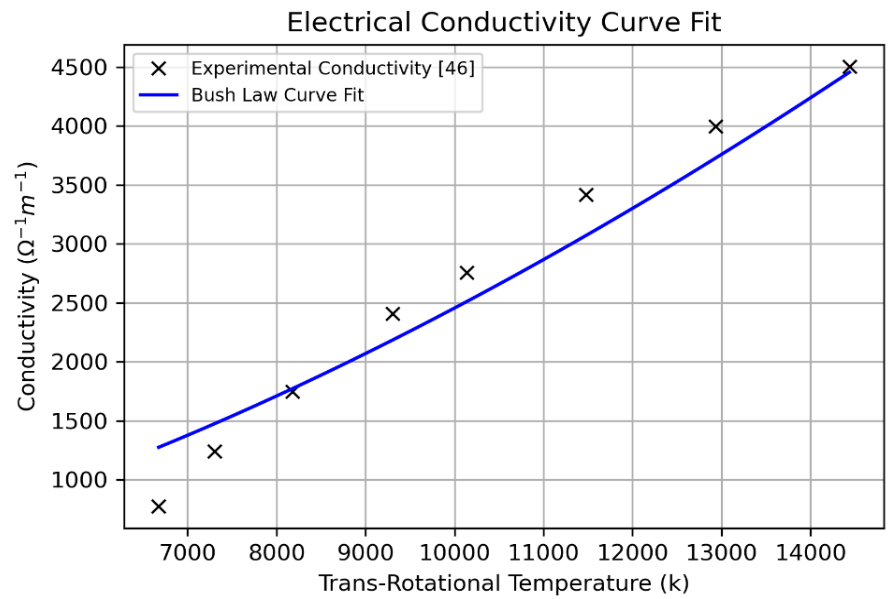

Chapman-Cowling

$$\sigma = A\frac{n_e}{\sqrt{T_{tr}}}.$$

Bush Model

$$\sigma = \sigma_0 \left(\frac{T}{T_0}\right)$$

$$\sigma_0 = 0.0008\ S/m$$

$$T_0 = 1.0\ K$$

$$n = 1.6218$$

Shear Stress

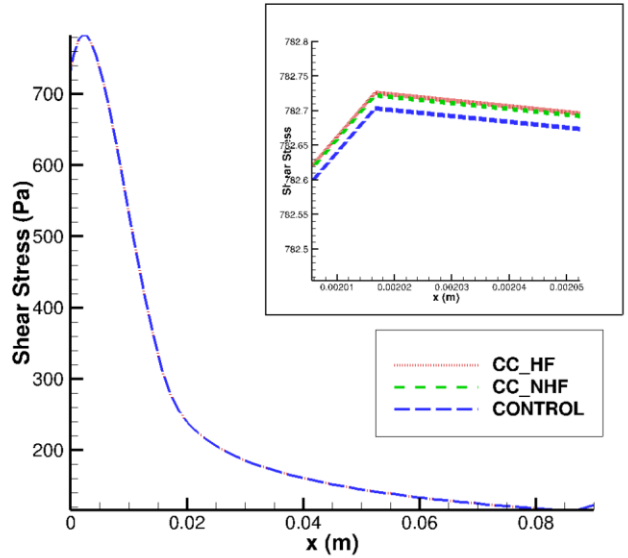

Magnetic Field

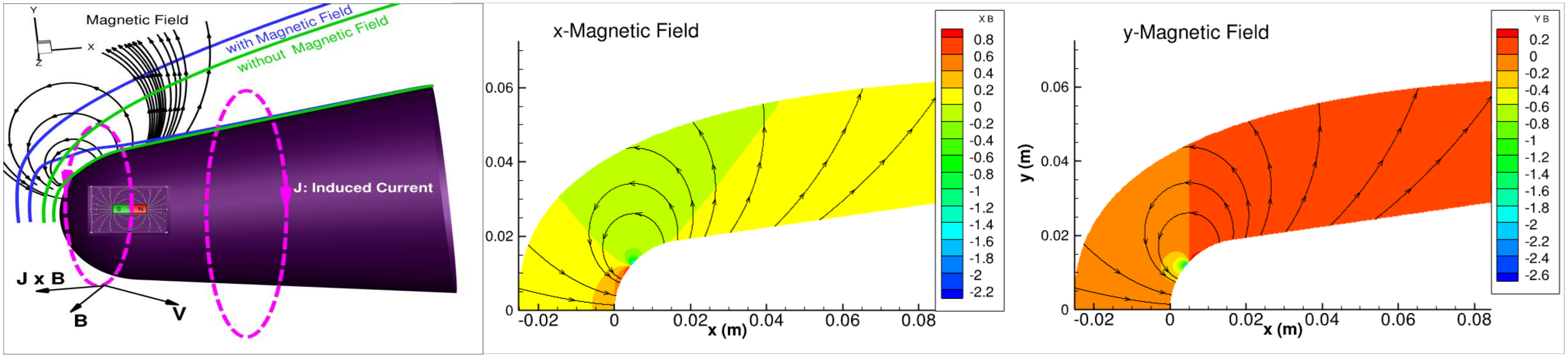

- An axisymmetric configuration is employed due to the nature of the problem.
- A **1T** magnetic field is introduced at the location **where the shear stress reaches** its maximum. The black lines on the left indicate the direction of the magnetic field.
- The spatial distribution of the *x*- and *y*-components of the magnetic fields is depicted.

Effect of MHD on Shock Structure

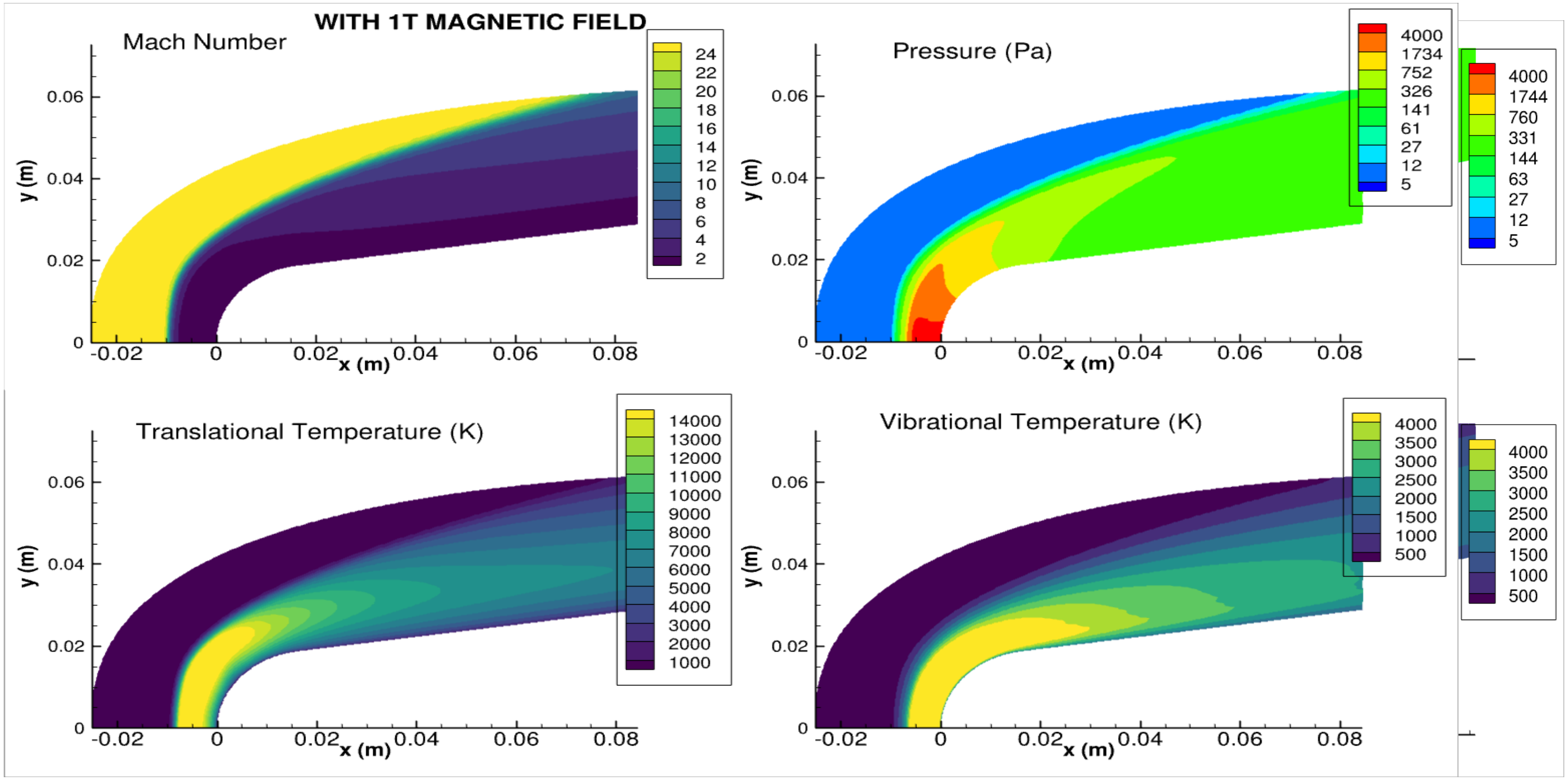

- The subsonic region near the wall enlarges.
- The pressure near the leading edge also increases.
- Both the translational and vibrational temperatures increase significantly.
- The **shock standoff distance increases** significantly under the influence of MHD.

Effects of MHD on Species Concentration

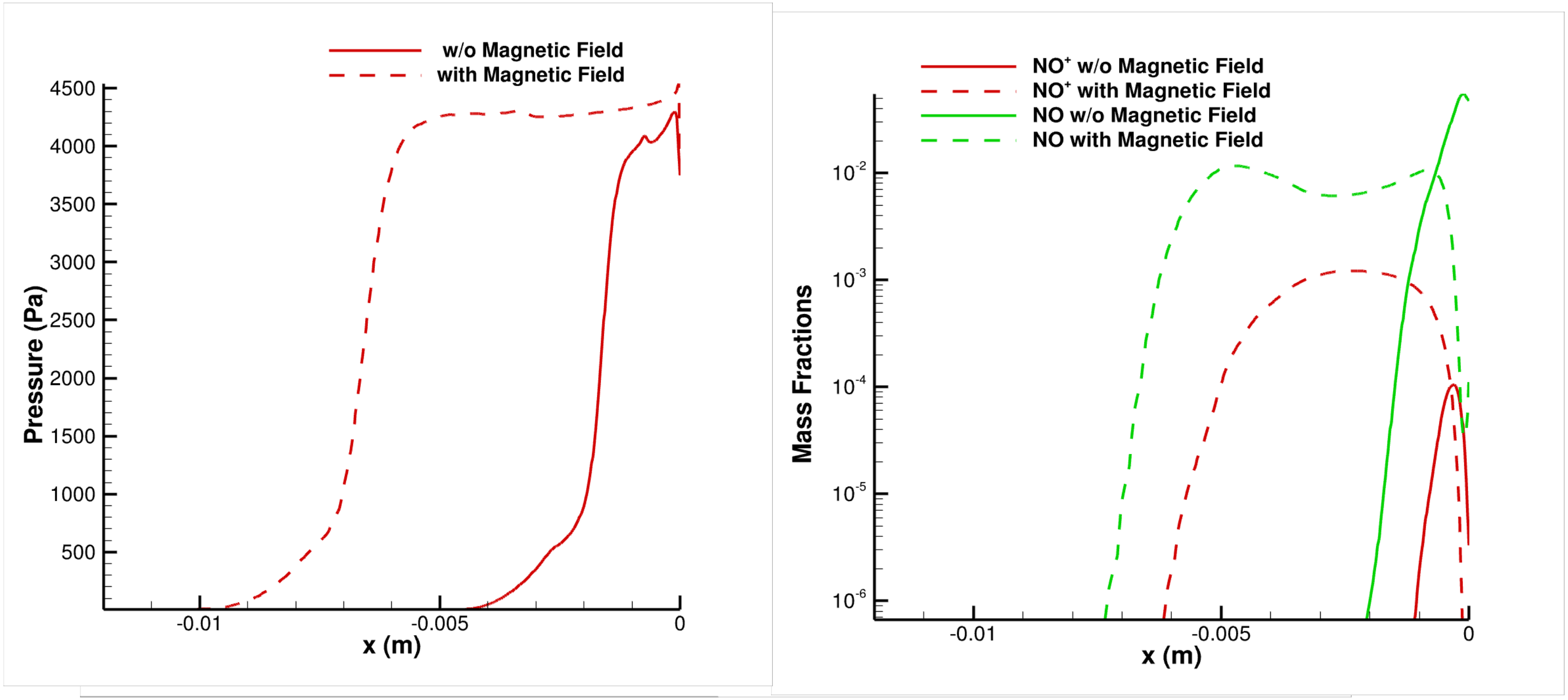

- NO molecules are **repelled** from the geometry.
- The pressure field increases significantly, especially near the leading edge.
- The concentration of NO+ increases by approximately two orders of magnitude.

Effects of MHD on Surface Parameters

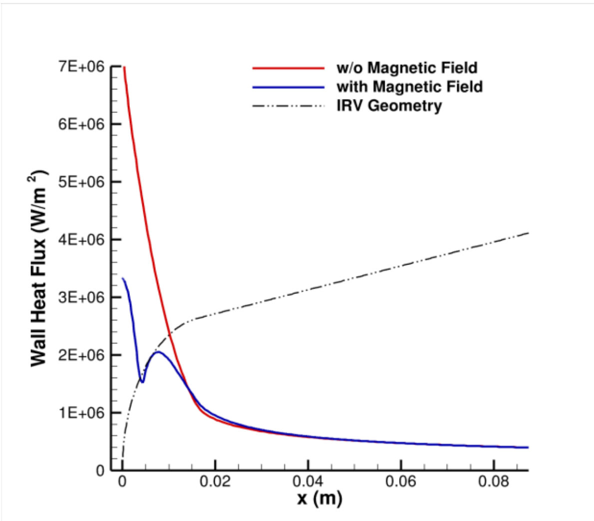

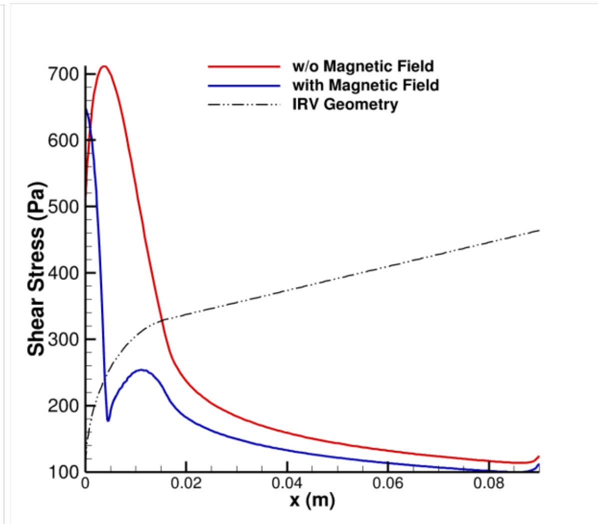

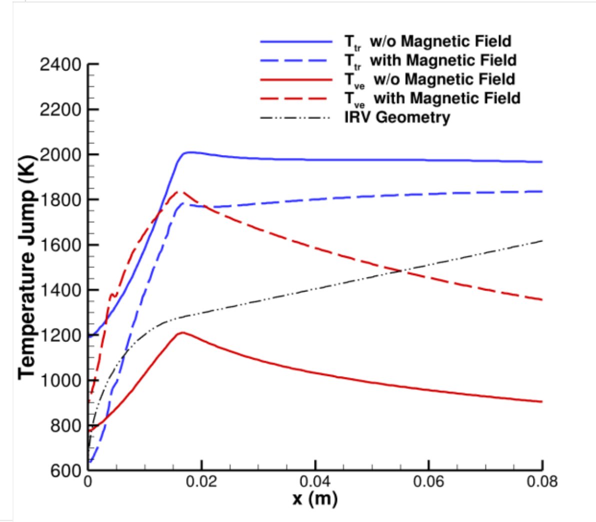

- The maximum **surface heating** value decreases by a factor of 2 with the presence of magnetic field. Similarly, the maximum shear stress reduces about 3 times.

- Both the wall heating and shear stress show a kink at the location where the magnitude of magnetic field is maximum.

- Due to the strong **nonequilibrium effects** the temperature jump in the translational mode decreases whereas the increases the vibrational mode.

Conclusions

- The presence of a magnetic field in the post-shock region significantly alters the flow field at high Mach numbers.
- The external magnetic field tends to reduce both thermal and shear stresses, thereby decreasing the overall thermal and mechanical loads on the vehicle.
- The mutual interactions among viscous stress, temperature fields, and electromagnetism are evident through reductions **in thermal flux** and **shear stress** in the weakly ionized post-shock plasma.
- Asymmetric changes in these loadings may serve as an **effective attitude control mechanism**, eliminating the need for internal hydraulics or other moving components.

Acknowledgements

- The author is thankful for the provision of computational resources from the Center for Computational Innovations (CCI) at Rensselaer Polytechnic Institute (RPI).

- The computational resources are granted by NSF-ACCESS for the projects of PHY240018 PHY240112 through Purdue's Anvil cluster.

- Financial support for this research was provided by RPI.

Thank you.